Check for updates

ARTICLE OPEN

Ultra-conformable liquid metal particle monolayer on air/ water interface for substrate-free E-tattoo

Fali Li[1,2], Wenjuan Lei[1,2], Yuwei Wang[1,2], Xingjian Lu[1,2,3], Shengbin Li[1,2], Feng Xu[1,2,3], Zidong He[1,2,3], Jinyun Liu[1,2,3], Huali Yang[1,2], Yuanzhao Wu[1,2], Jie Shang[1,2], Yiwei Liu[1,2,3 ✉] and Run-Wei Li [ID][1,2,3 ✉]

Gallium-based liquid metal has gained significant attention in conformal flexible electronics due to its high electrical conductivity, intrinsic deformability, and biocompatibility. However, the fabrication of large-area and highly uniform conformal liquid metal films remains challenging. Interfacial self-assembly has emerged as a promising method, but traditional approaches face difficulties in assembling liquid metal particles. Here, we realized the multi-size universal self-assembly (MUS) for liquid metal particles with various diameters (<500 μm). By implementing a z-axis undisturbed interfacial material releasing strategy, the interference of gravitational energy on the stability of floating particles is avoided, enabling the fabrication of ultra-conformable monolayer films with large areas (>100 cm^2) and high floating yield (50–90%). Moreover, the films can be conformally transferred onto complex surfaces such as human skin, allowing for the fabrication of substrate-free flexible devices. This eliminates interference from traditional substrate mechanical responses, making the liquid metal e-tattoo more user-friendly.

INTRODUCTION

With the increasing demand for the integration of electronic devices into the human body, ensuring conformity has become increasingly crucial in guaranteeing reliable operations[1–3]. However, due to the non-developable surface of the human body and the complex deformation it experiences in daily life, flat flexible devices face instability and discomfort when working in the complex mechanical environment on human skin[4–6]. As a result, tattoo-like electronic devices have become a trending solution due to their comfort and user-friendliness[7–10]. Gallium-based liquid metals, with their intrinsic deformability[11,12], outstanding electrical properties[13,14], and good biocompatibility[15–17], have emerged as promising candidates for fabricating conformal electronics[13,14]. Based on liquid metal particles[18,19], a variety of flexible devices have been developed for detecting physiological signals of the human body, and the conformity of these devices has also improved[20,21]. Nevertheless, despite being widely used in flexible electronics, it remains challenging to fabricate large areas of a uniform conformal liquid metal film.

Interfacial self-assembly is a competitive candidate for developing conformal liquid metal film. Widely adopted in various fields, this technique enables the fabrication of monolayers composed of diverse nanomaterials, including metallic nanoparticles and nanowires[22,23], carbon-based nanomaterials[24], and organic nanomaterials[25]. In contrast to conventional methods for producing conformal devices, such as substrate sacrificial transferring, the interfacial self-assembled film is more amiable to complex surfaces[26–29]. Thus, its application in preparing conformal liquid metal films holds considerable appeal.

However, traditional interfacial self-assembly methods are mainly applicable to nano-sized materials[30–33], it has difficulties in assembling liquid metal particles, which are relatively large-size (<500 μm) and high density (~6g cm^{-3}). From a theoretical standpoint, the surface tension of water exhibits a sufficiently high magnitude to uphold liquid metal microparticles at the air-water interface[34]. However, this equilibrium can be effortlessly disrupted by the kinetic energy that is amassed during the interfacial self-assembly process.

Here we propose a multi-size universal self-assembly (MUS) strategy for fabricating liquid metal particles monolayer (LMPM). The monolayer can be transferred conformally from the air-water interface onto a wide range of substrates. To mitigate interference factors associated with traditional methods, we introduce a z-axis undisturbed material-releasing strategy. Under the influence of the Marangoni force, liquid metal particles can diffuse to the interface when the slurry of liquid metal particles and alcohol contacts the air/water interface. In this process, interference factors in the vertical direction are eliminated, allowing the liquid metal particles to float and assemble more efficiently at the air-water interface. Benefitting from this improvement, the MUS demonstrates its universality in various sizes and compatibility with LMPs of diameters ranging from hundreds of microns. This advancement lays the foundation for a universal and more effective method for obtaining large-area and uniformly conformal liquid metal film and further fabricating it into large-area conformal devices.

RESULTS AND DISCUSSION

Theoretical analysis of the floating mechanism of liquid metal particles

The stability of particles on an interface is theoretically maintained by kinetic energy barriers, as described by Young's equation(Eq. (1))[34]. The contact angle for a particle at equilibrium depends on the interfacial tensions at particle-air, γ_{pa}, particle-liquid, γ_{pl}, and air-liquid, γ_{al}. If the particle detached from the

[1]CAS Key Laboratory of Magnetic Materials and Devices, Ningbo Institute of Materials Technology and Engineering, Chinese Academy of Sciences, Ningbo 315201, P. R. China. [2]Zhejiang Province Key Laboratory of Magnetic Materials and Application Technology, Ningbo Institute of Materials Technology and Engineering, Chinese Academy of Sciences, Ningbo 315201, P. R. China. [3]College of Materials Science and Opto-Electronic Technology, University of Chinese Academy of Sciences, 100049 Beijing, P.R. China. ✉email: liuyw@nimte.ac.cn; runweili@nimte.ac.cn
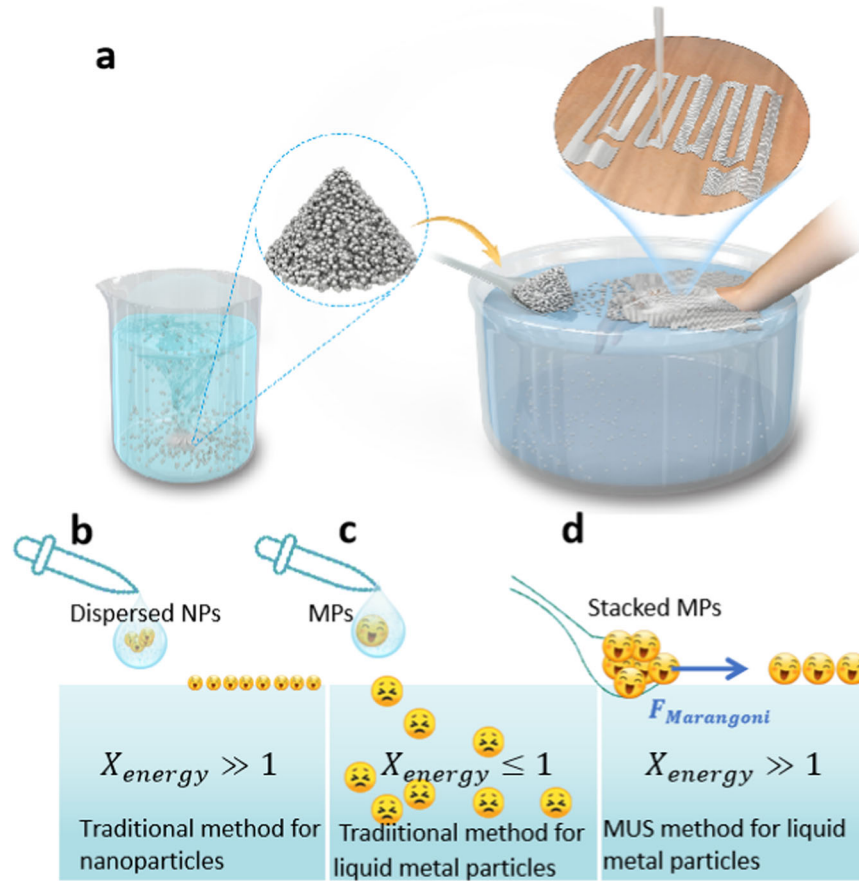
Fig. 1 Schematics of multi-size universal self-assembly (MUS) for liquid metal particle monolayer (LMPM). a The schematic diagram of fabricating liquid metal based conformal circuits. Mainly includes following steps: pre-dispersion of liquid metal particles, particle releasing at the interface, particles self-assembling into monolayer, and conformal transferring of LMPM. **b** The self-assembly of nanoparticles by traditional method. **c** Traditional method failed to assemble micro-scale liquid metal particles. **d** The self-assembly of liquid metal microparticles by MUS method.

interface and is submerged into the liquid phase, the free energy ΔG to be overcome to submerged is shown in Eq. (2)[34]. In the conventional assembling process, a colloidal droplet falls at a specific height h. Here we can define a parameter X_{energy} in Eq. (3), which is the ratio of free energy (ΔG) and kinetic energy (ΔE) accumulated in the falling process. Taking the liquid metal microparticles floating on water as an example, we can get Eq. (4). (for numerical details, see the supporting materials)

$$\cos\theta = \frac{\gamma_{pa} - \gamma_{pl}}{\gamma_{al}} \quad (1)$$

$$\Delta G = \pi r^2 \gamma_{al}(1 - \cos\theta)^2 \quad (2)$$

$$X_{energy} = \frac{\Delta G}{\Delta E} = \frac{3\gamma_{al}(1 - \cos\theta)^2}{4r\rho gh} \quad (3)$$

$$\text{For liquid metal} : X_{energy} \leq \frac{1.75 \times 10^{-5} m}{r} \quad (4)$$

Consequently, a larger particle yields a smaller value of X_{energy}, thus decreasing particle stability in the assembling process. For metallic particles, it's easier to be disturbed by the kinetic energy when the radius exceeds a specific value (17.5 μm for liquid metal), thus making it difficult to assemble into a film at the air-liquid interface. X_{energy} is the crucial parameter that determines the practicability of the interfacial assembly for large-size materials.

The above section describes the research on the stability of LMP at the air/water interface, while the dynamic process of its diffusion has been relatively clear in previous studies. At the interface between alcohol and water, Marangoni forces arise due to the difference in surface tension between the two liquids. Under this effect, LMP will move from alcohol to water, and the direction of the force on the particles determines their trajectory, which in turn determines whether the particles ultimately float on the water surface or sink into the water (see Supplementary Fig. 4i–j for details).In the MUS process, we eliminated the pre-step of uniformly dispersing the particles, and instead directly started from the micro-particles' precipitate in ethanol. The micro-particles in precipitation are released horizontally when contacting the air-liquid interface, and the Marangoni force mediates the process. Therefore, by decreasing the particles' kinetic energy in the vertical direction, this method can reduce the X_{energy} and thus enable the interfacial self-assembly of liquid metal micro-particles.

To elucidate the benefits of utilizing the MUS strategy in detail, a comparative analysis is presented in Fig. 1b–d. Firstly, with regard to the nanomaterials employed in the traditional interfacial self-assembly method, it is evident that $X_{energy} \gg 1$, resulting in the facile and homogeneous dispersion of the material in ethanol, thereby forming a colloidal solution. The dropwise addition of this solution to water expeditiously yields a monolayer at the air-liquid interface. On the contrary, as illustrated in Fig. 1c, micro-scale metallic materials pose a significant challenge when attempting to maintain stable dispersion in ethanol. In contrast, as shown in Fig. 1b, micro-scale metallic materials are difficult to disperse
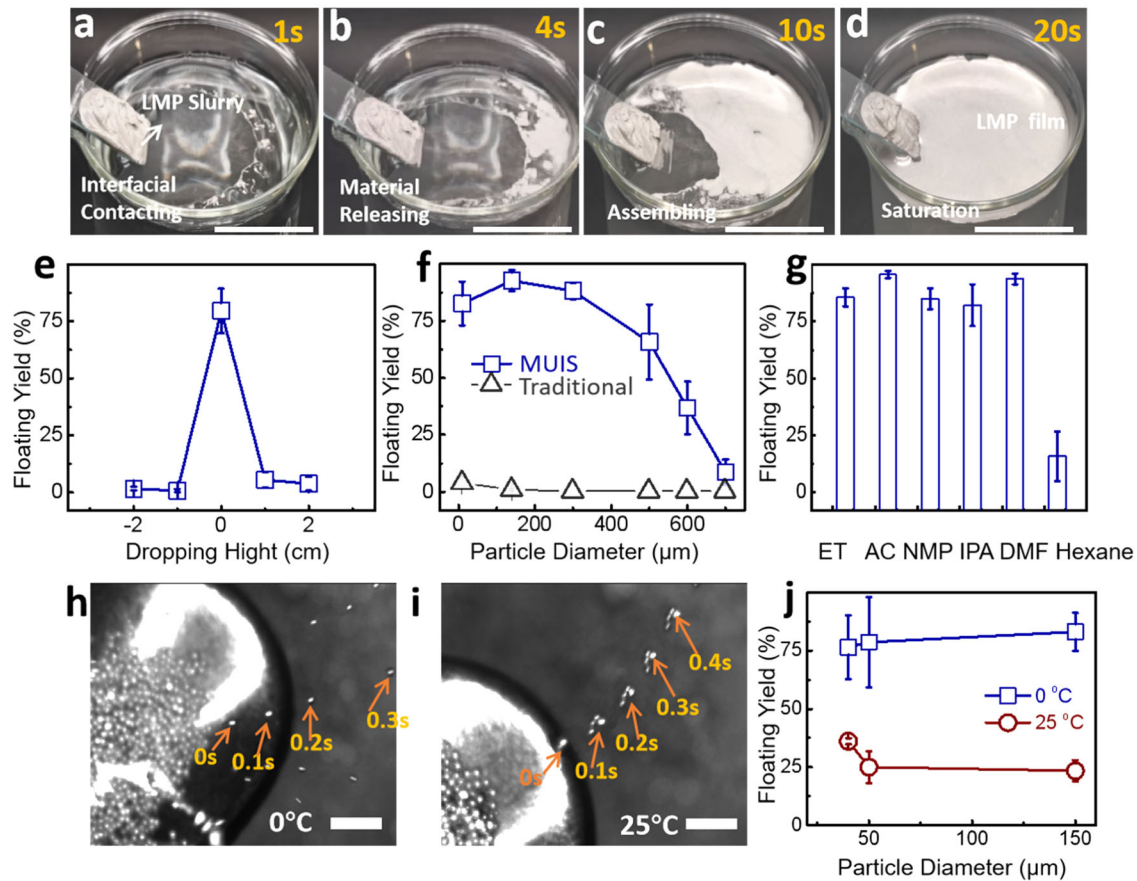
Fig. 2 Fabrication of liquid metal micoparticle monolayer. a–d Photographs of different steps in MUS. Scale bars, 5 cm. **e** The floating yield according to dropping height of liquid metal slurry(error bars: standard deviation). **f** Floating yield of the traditional method (dropwize adding) and MUS method according to the diameter of liquid metal particles(error bars: standard deviation.). **g** Floating yield of liquid metal particles based on different water soluble solvent (ethanol, acetone, n-methylpyrrolidone, n-dimethylformamide, isopropyl alcohol) and water insoluble solvent (hexane)(error bars: standard deviation.). **h, i** Time-lapse microscopic photographs of the liquid metal particles in the "material releasing" process taken at 0 °C and 25 °C, respectively. Scale bars, 500 μm. **j** Floating yield of liquid metal particles according to the temperature(error bars: standard deviation).

stably in ethanol. In the process of adding this suspension to the water, the prerequisite condition of $X_{energy} \gg 1$ is no longer holds. Therefore, the microparticles are unstable at the gas-liquid interface. Disturbance such as kinetic energy accumulated during the falling process of droplets, can easily break this balance and cause the material to sink into the water. Taking the above considerations into account, the MUS is shown in Fig. 1d. This method does not need to disperse the material uniformly in ethanol, and can directly utilize the precipitation of particles. When the residue is positioned at the interface between air and water, it can prompt Marangoni forces owing to the distinct surface tension between ethanol and water[19]. Such forces can extract the particles from the condensed precipitate and extend them across the interface. Since the force is parallel to the in-plane direction, and the interference factor (gravity) in the vertical direction is effectively evaded, the micro-particles are relatively stable and do not sink. Additionally, the micro-particles become densely packed at the interface, forming a monolayer.

The schematic diagram of the MUS is shown in Fig. 1a, which encompasses four stages, namely precipitate preparation, interfacial self-assembly, conformal transfer, and film processing. Initially, the liquid metal particles are agitated thoroughly in ethanol, following which a slurry of liquid metal particles is obtained upon settling for a few minutes. This slurry is then brought into contact with the air-water interface. The Marangoni effect is induced by the difference of surface tension between the

ethanol and water, which will cause Marangoni flow from the slurry to the interface. This flow causes the liquid metal particles to diffuse alongside the ethanol to the air-water interface, where they undergo self-assembly to form a monolayer. Furthermore, the particle film can be easily transferred to complex surfaces such as the human body. Finally, a conformal liquid metal particle film is obtained, which can be utilized for fabricating flexible circuits and sensors via techniques like mechanical sintering.

The MUS method exhibits a time-saving advantage in fabricating LMPM. Figure 2a–d shows the film preparation process (details shown in Supplementary Video 1). The film was prepared within the 20 s (diameter ≈ 10 cm). In Fig. 2a, a glass slide is used to carry the liquid metal slurry to contact the air-water interface. It can be seen that the particles form a flower-like pattern under the action of the Marangoni force. As the liquid metal particles diffuse into the air-water interface, the film shows up in the right of the beaker and saturates at 20 s (Fig. 2b–d). After removing the slurry, the LMPM covers the entire air-water interface.

Self-assembly and conformal transfer of liquid metal particle films

The influencing factors on the film preparation are systematically studied in Fig. 2e–j. The self-assembly process is greatly affected by particle size. Standard methods like ultrasound and stirring produce liquid metal particles with relatively dispersed sizes, making it difficult to explore the correlation between particle size

and the assembly process. Therefore, it is necessary to first prepare monodisperse liquid metal particles. This is achieved using the microtube spraying method, as shown in Supplementary Fig. 3a, to obtain monodisperse liquid metal microparticles. A glass microtube is employed to exert high pressure on liquid metal, causing the bulk liquid metal to contract and form microparticles. The diameter of the liquid metal particles can be easily controlled by controlling the diameter of the glass microtubes (shown in Supplementary Fig. 3b).

In the previous theoretical analysis section, by defining the stability parameter X_{energy}, we predicted the vast impact of particle kinetic energy (vertical) on particle floating stability. Here, monodispersed liquid metal micro-particles (diameter ≈ 30 μm) are taken as an example to experimentally demonstrate the importance of controlling the height of particle release. As shown in Fig. 2e, it is difficult to achieve particle flotation and assembly when releasing above or below the water surface. In contrast, liquid metal particles can efficiently float and assemble by releasing liquid metal at the interface. However, due to the incompatibility of liquid metal microparticles with the traditional method, almost no films are obtained at the interface. Figure 2f compares the flotation yields of liquid metal particles with a size distribution of 10–700 μm using both the traditional method and the MUS method. In contrast, the MUS method is effective for micron-sized liquid metal particles. For particles with diameters below 300 μm, the film yield is above 75%. Although this method improved a lot compared to the traditional way, it is still challenging to achieve 100%. Supplementary Fig. 4 may provide some explanation for this. Here we can define two kinds of liquid metal particles, A and B, and both can diffuse into the interface from the slurry. B maintains a relatively constant speed and finally moves to the far side of the interface to assemble into a film, while A drops rapidly after a short distance. Supplementary Fig. 4i shows schematic diagrams of force analysis for two types of particles. The different force directions at the interface for particles A and B result in different subsequent trajectories. The force direction on particle B remains in the horizontal direction (or with a very small vertical component), which leads to its final stable position at the air/water interface. In contrast, particle A sinks to the bottom due to the excessive force acting in the vertical direction.

As the particle diameter exceeds 500 μm, the effect of gravity becomes increasingly prominent, leading to a decrease in floating yield with an increase in diameter. For a size of 700 μm, even if the liquid metal particles can float on the interface by the MUS process. However, it is unstable and prone to falling into the water under gravity. Further, the method is not limited to the use of alcohol as the pre-dispersed phase of the particles. The effect of the different solutions on the MUS process was also tested (Fig. 2g). Unlike water-insoluble solvents (hexane), when using other water-soluble organic solvents (such as acetone, NMP, and DMF), it can also achieve high film yields (>75%).

As the melting point of liquid metal is close to room temperature, the temperature of the ambient environment can also impact the MUS process. The time-lapse microscopic paragraph of the diffusion process at 0 °C is shown in Fig. 2h. At this temperature, the liquid metal particles are solidified. From the trajectory of a single particle, we can see no adhesion between particles during the material-releasing process. In contrast, when the temperature reaches 25 °C, the interior of particles presents a liquid state, and the oxide skin maintains its shape. Influenced by the adhesion of the oxide skin, the particles aggregate and are closely packed. The temperature also significantly influences the floating yield of the self-assembled particle film, as shown in Fig. 2j. With increasing temperature, the particle floating yields reduced. Therefore, for lower melt point materials, temperature plays an important role in the film yields when using the MUS method.

The morphology of LMPM is examined using liquid metal particles of varying diameters, as illustrated in Fig. 3a–f. From the top view in Fig. 3a–c, it can be seen that the liquid metal particles are arranged in a close-packed state, and their diameters are about 150 μm, 40 μm, and 30 μm, respectively. Figure 3d–f depict a cross-sectional view of the film, revealing that it comprises a solitary layer of liquid metal particles. The thickness of this layer corresponds to the diameter of each individual particle. Except for liquid metal, we further explored the universality of the MUS method on other materials. Here we choose three representative materials, which are common metal (copper), magnetic material (FeSiB), and compound (ZnS). Supplementary Fig. 5a–c shows the optical photos of the self-assembled particle films obtained by the MUS method for three kinds of particles, respectively. Supplementary Fig. 5d–i shows the microscopic images of the above three microparticle films. Based on the cross-sectional analysis of SEM images presented in Supplementary Fig. 5g–i, it can be inferred that the films consist of a singular layer of particles, and that the thickness of the films is uniform and equivalent to the diameter of each individual particle.

The electrical properties of the liquid metal film are shown in Fig. 3g, h. The mono-disperse liquid metal particles used to obtain the LMPM at the air-water interface have an average size of 30 μm. Then, the film is transferred to the PDMS substrate, and the sample size is 1×4 cm. The initial resistance of the sample fluctuates around 10^6 Ω, as shown by the black line in Fig. 3g. The maximum strain for the first cycle is set at 20%. During the strain loading process, the resistance is always in the 10^6 Ω until the strain exceeds a certain threshold (about 18%), suddenly drops to near 10^5 Ω, and remains relatively stable in the unloading process. In the following tensile cycle, the maximum strain increases to 30%, 40%, and 50%, corresponding to the dark blue, blue, and light blue curves in Fig.3g, respectively. When the strain of the monolayer exceeds the highest strain in history, its resistance will begin to decline until the resistance reaches the order of 10 Ω. We speculate that this phenomenon is caused by particle breakage and conductive path formation during stretching[35]. In Supplementary Fig. 7, SEM images of the thin film are shown before stretching, after 1, 100, and 10,000 stretches, respectively. It can be observed that after undergoing strain from stretching, the liquid metal particles are no longer separated from each other. The oxide layer between the particles is disrupted during deformation, allowing the liquid metal to connect with each other and form conductive pathways, resulting in a rapid decrease in thin film resistance.

The subsequent cyclic tensile test can also support this view (Fig. 3h). The sample is stretched for 1000 cycles with maximum strain at 50%. In the first cycle, the resistance rapidly decreases from the 10^6 Ω to the magnitude of 10 Ω, and becomes relatively stable in the subsequent process (long-term performance under 10000 cycles also shown in Supplementary Fig. 13). Inset shows the details of resistance changes after hundreds of stretching exercises. The initial resistance is 3.18 Ω, which decreases with the increase of strain and recovers with the unloading of strain. The anomalous strain-resistance relationship exhibited in materials based on liquid metal particles has been explained in related studies[35]. In this paper, we will draw upon the theory presented in ref. [35] to explain this phenomenon. The conductive pathways in the film are formed by serially connected spherical particles, with non-uniform thickness in the vertical direction, resulting in protrusion structures at the center of the particles (as shown in Supplementary Fig. 7). Therefore, under tensile strains less than 100%, the liquid metal stored inside the protrusions will gradually extend to other locations (such as the neck position at the particle connections) as the strain increases, enhancing the overall conductivity.

The LMPM can be conformally transferred to complex surfaces, which is the base of conformal flexible electronic devices. As an
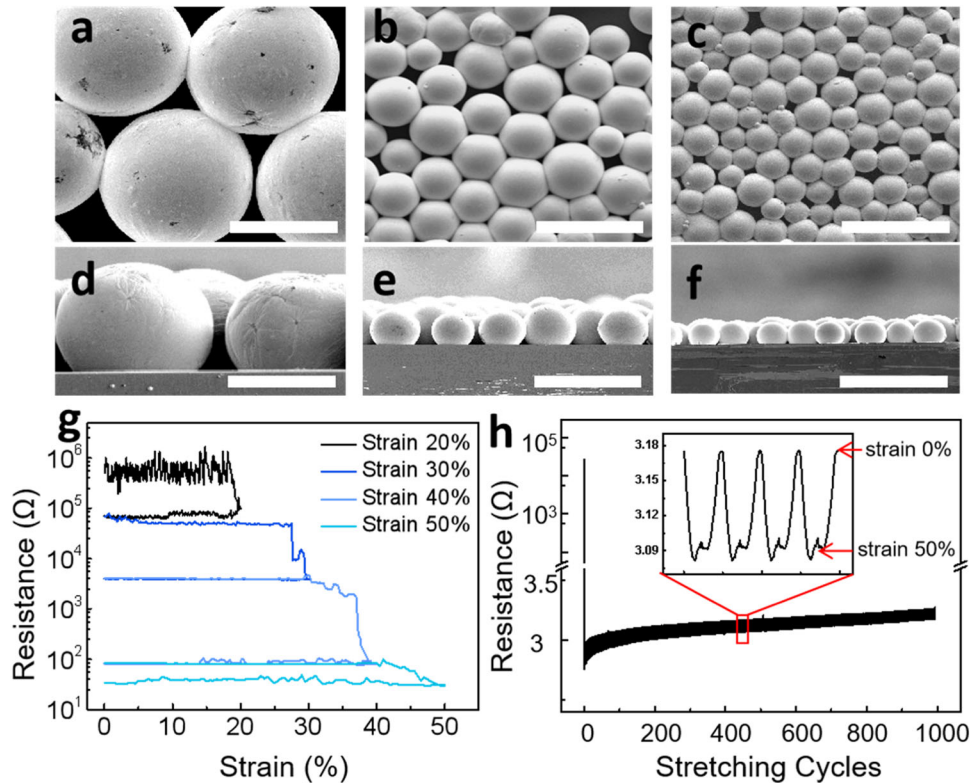
Fig. 3 The surface topography and electrical property of LMPM. a–c SEM images of LMMM with different diameters (150 μm, 40 μm and 30 μm, respectively). Scale bars, 100 μm. **d–f** Cross-sectional SEM images of the liquid metal monolayers in Fig. 3a–c. Scale bar: 100 μm. **g** Resistance of liquid metal monolyer (particles diameter: 30 μm) under different strain and the size of sample is 1 cm × 4 cm. The maximum strain of the first cycle is 20%, then gradually increases by 10% until reaches 50%. **h** The resistance of LMPM as the function of stretching cycles. The size of sample is 1 cm × 4 cm.

example, we use the LMPM based on liquid metal particles of 30 μm to demonstrate its conformal ability. Lift-off approach is adopted in the film transfer process. As shown in Fig. 4a, the object (a volumetric flask) is first placed underwater and then pulled out of the water. During the lifting step, the LMPM automatically conformal covers the surface. The LMPM can be effectively transferred to flat objects (silicon wafers, Fig. 4b), and elastic spheres (silicone hemispheres, Fig. 4c). The deformability of the film on the PDMS substrate is shown in Fig. 4d. Under 50% tensile strain, the film does not seem to detach. The film is further transferred to an uneven surface, such as the cherry leaf (shown in Fig. 4e). Despite the intricate microstructure of the leaf, the liquid metal particle film demonstrates a remarkable conformal solid capability. Figure 4f, g shows the SEM image of LMPM on a cherry leaf. It can be seen that the liquid metal particles can cover the undulating structures such as the veins of the leaf. In addition to uneven surfaces, liquid metal particle films can also be transferred to complex three-dimensional curved surfaces. The conformal attachment of LMPM to the surface of nitrile gloves is shown in Fig. 4h, i. Based on the front and back images of the glove, we can infer that the liquid metal particle film has fully covered the entire surface. Compared with nitrile gloves, the surface of the human finger has a more complex wrinkle structure. Figure 4j shows the LMPM transferred to the back of the finger, which is conformally attached to the skin (details shown in Supplementary Video 2). Furthermore, as depicted in the inset, the film can be transferred onto a fingerprint while preserving its original structure.

Conformal liquid metal flexible electronic devices
The conformal liquid metal particle film is essential for further obtaining conformal liquid metal-based flexible electronic devices.

Supplementary Fig. 10 demonstrates the patterning of LMPM and the circuit fabricating based on it. To begin, the mask (composed of paper) is affixed to the object. Next, the target object is submerged into water, and upon removal, the film adheres to the surface of the object. Subsequently, pressure is applied to the film using a brush to activate the liquid metal particles and create a conductive pathway. Finally, removing the mask allows for the patterning of the LMPM onto the surface of the three-dimensional object.

The conformal LMPM depicts potential as a conformal heater in skin electronics. Local heating of the lesion area is a common health care measure in daily life, and the key is achieving conformal contact with the lesion area. Figure 5a demonstrates the conformal heating function of the LMPM on a prosthesis surface with raised structures simulating human skin lesions, using paraffin as a simulation material. In Fig. 5b, LMPM is conformally transferred to the surface of the lesion area. The projection of this area is a circle with a diameter of 1.5 cm, but its three-dimensional structure is relatively complicated. The inset of Fig. 5b (side view) shows that the LMPM achieves conformal coverage of this region. It is worth mentioning that the film is straightforward to wash off after use. Figure 5c shows the LMPM deposited on the joints of the author's hand. The film doesn't fall off during the normal movement of the human palm. But it can be easily washed off by soap in 1 min (Fig. 5d).

The conformal heating process is demonstrated in Fig. 5e–g. A low-voltage, high-frequency inductive heating device is positioned near the LMPM. The high-frequency electric field induces eddy currents in the metal film on the skin, resulting in the production of Joule heat. The temperature can be controlled by controlling the heating time and the distance between the induction coil and the skin. The infrared picture of the hand is
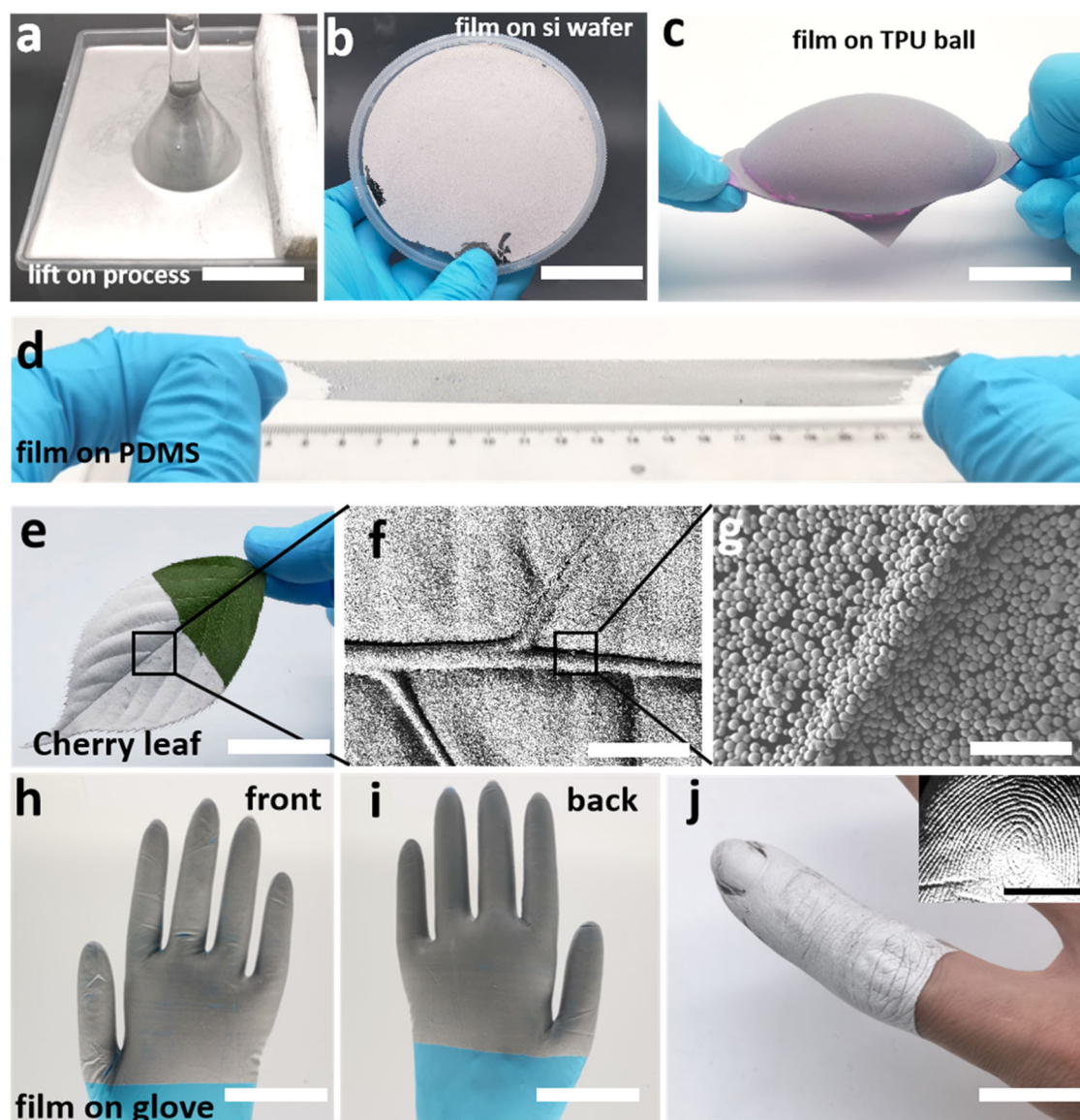
Fig. 4 The Conformal transfer of LMPM to various surfaces (flat, curved, complex). a The Conformal transferring process of LMPM from the air-water interface to the surface of a glassware. Scale bars: 10 cm. **b, c** Photographs of LMPM transferred to silicon wafer and silicone hemisphere. Scale bars: 4 cm, 2 cm. **d** Photograph of the LMPM transferred to PDMS, which is being stretched with the strain of 100%. **e**–**g** Optical and SEM images of LMMM transferred to the surface of cherry leaf. Scale bars: 3 cm, 2 mm, 500 μm. **h, i** Optical photographs of self-assembled liquid metal films on the surface of gloves, front and back, respectively. Scale bars: 5 cm. **j** Optical photograph of LMPM on the index finger. Scale bar: 2 cm. Inset: Microscopic image of the film on the fingerprint. Scale bar: 500 μm.

shown in Fig. 5f (heating for 10 s). The temperature at the location of the blue curve in Fig. 5f and the height at the location of the black curve in Fig. 5b are extracted and displayed in Fig. 5g. It can be seen that although the morphology of the lesion fluctuates greatly, the temperature maintains high uniformity. Uniform and precise heating of specific locations on the skin is achieved.

In addition, we have utilized the patterned conformal LMPM to fabricate flexible devices on both human skin and plant leaves (Fig. 5h–m). The conformal flexible circuits remained stable and functional even when the finger was bent, straightened, or underwent other movements that resulted in changes in the wrinkle pattern on the skin (Fig. 5h, i). Furthermore, the luminosity of the red LED remained consistent, further indicating the stable performance of the device (details shown in Supplementary Video 3). Figure 5j shows a conformal liquid metal-based strain sensor fabricated on the back of the thumb. There is no additional substrate between the sensor and the skin, so the interference

from the mechanical properties of the substrate can be reduced. The resistive signal of the conformal sensor was continuously tested during continuous thumb movement (Fig. 5l).

During the vigorous thumb movement, the conformal film exhibited remarkable adhesion to the human skin without any detachment or breakage, thus verifying the exceptional adhesive ability of the liquid metal film. LMPM is also transferred to the leaf and patterned to obtain strain sensors. The use of the object under test as a substrate for sensor fabrication provided greater flexibility and reduced the constraints of the flexible substrate. During the entire experiment, the growth of the leaves is not disturbed by the sensor. Figure 5m shows the data obtained by continuous monitoring for 20 days. In the first ten days, the leaf growth is slow due to cloudy weather, but in the next ten days under strong light conditions, the leaf grows rapidly, and the resistance of the strain sensor also increases quickly. In summary, the conformal flexible electronic device based on LMPM could
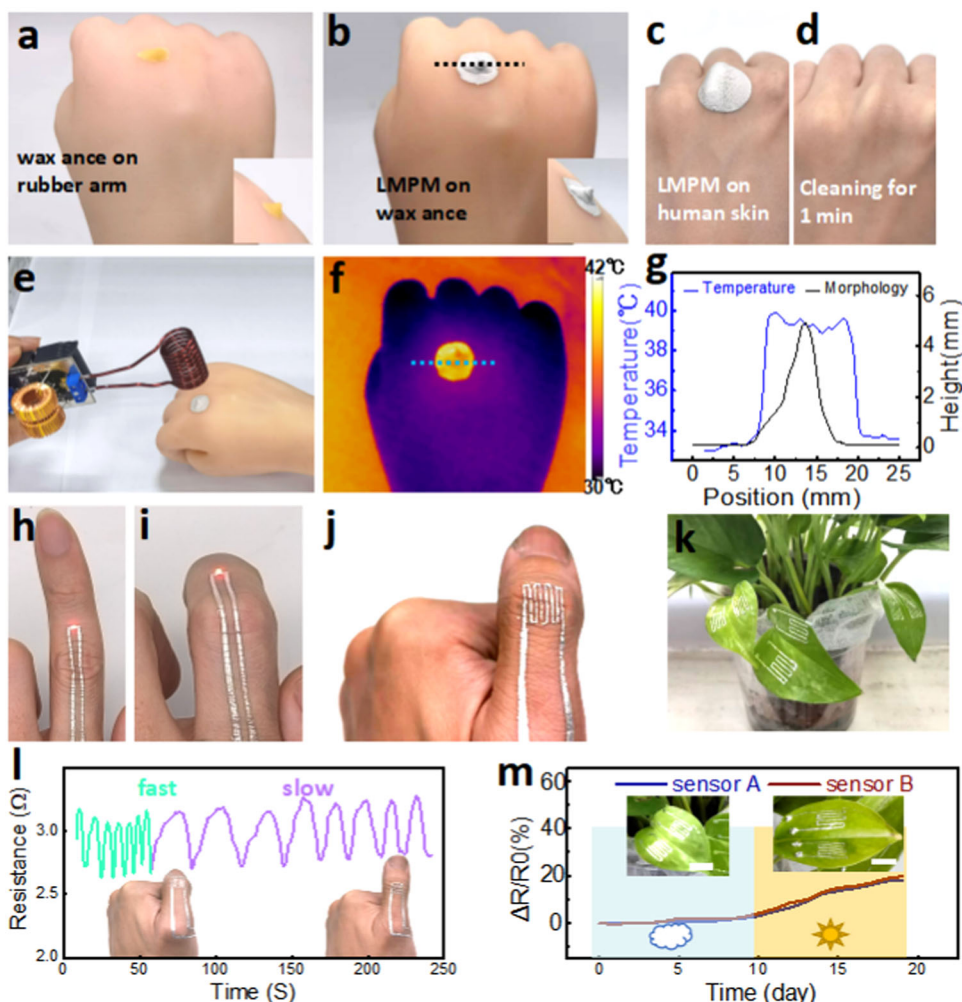
Fig. 5 liquid metal E-tattoo on human skin as wireless conformal heater and conformal flexible circuits and sensors. a Wax is used to construct a raised structure on the surface of the silicone prosthesis, which simulates the structure of human skin lesions. **b** The LMPM is transferred to the "lesion site" to achieve conformal coverage of this structure. **c, d** LMPM transferred to the joints of human skin, which can be completely removed after a one-minute soap washing step, leaving the skin clean without residue. **e** Non-contact heating of conformal LMPM is achieved using a commercial high-frequency low voltage induction heater. The temperature is controlled by controlling the time and distance between the induction coil and the film. **f** Infrared image of the prosthetic skin after ten seconds of heating. (**g**)The contrast of height and temperature where the lesion is located. Corresponding to the position of the black dotted line in Fig. 5b and the position of the blue dotted line in Fig. 5f, respectively. **h, i** The conformal liquid metal circuit located on the back of the finger. **j** The conformal strain sensor on the back of the thumb. **k** The conformal strain sensor on the leaf of epipremnum aureum. **l** The curve of strain sensor's resistance versus time. The strain sensor is located at the back of thumb which makes the flexing-stretching motion. **m** The resistance change of strain sensor during leaf growth. The plants were in the shade for the first ten days, and were exposed to sunlight or artificial light for the next ten days.

precisely reflect the actual state of the measured object without substrate constraints, thereby offering immense potential for various applications.

In summary, the self-assembly of liquid metal particles into large-scale (>100 cm^2) monolayers at the air-water interface has been investigated for the development of ultra-conformal E-tattoos. Benefiting from the shielding of interference from gravity in the MUS method and the assistance of Marangoni force, both nano to micro-sized (<500 μm) liquid metal particles can be self-assembled into monolayer in the air-water interface. The monolayer can be conformally transferred to silicon wafers, spherical surfaces, human skin, etc., and other complex surfaces. Based on this conformal liquid metal film, flexible circuits and sensors have been prepared on human skin, demonstrating conformal ability and adherence to complex structures without foreign body sensation. The E-tattoo does not interfere with the measured object, making it user-friendly without substrate limitation. Furthermore, it does not hinder the movement of the

human body and growth of plants.The ultra-conformal liquid metal monolayer provides a valuable tool for further research in conformal flexible circuits, wearable sensors, and other device applications.

METHODS

Preparation of liquid metal and liquid metal microparticle

Gallium (99.99%; Beijing Founde Star Sci. & Technol. Co., Ltd), indium (99.995%; Beijing Founde Star Sci. & Technol. Co., Ltd), were mixed together in the ratio of 3:1 by mass. Then the mixture was heated and stirred for 30 min protected by nitrogen at 60 °C to obtain liquid-metal EGaIn (Ga75In25). The preparation of liquid metal particles utilizes a self-made high-pressure micro-pipe injection device. The liquid metal is injected into the dispensing syringe, and high-pressure nitrogen is introduced into the rear to force it through the micron glass tube. By controlling the diameter of the glass tube, monodisperse liquid metal particles of different

sizes were obtained. The obtained liquid metal microparticles are cryopreserved to prevent interparticle agglomeration.

Preparation of other micron materials

Zinc sulfide microparticles were purchased from Shanghai keyan materials. The copper micro-particles and FeSiB micro-particles were purchased from Zhongnuo New Materials, and a metal screen was used to control their particle size uniformity.

Preparation and conformal transferring of self-assembled particle films

The following content takes liquid metal as an example, and the operations for other materials are the same. The liquid metal particles were stirred in alcohol for 10 min (ice bath, temperature below the melting point of the liquid metal). After standing for 5 min, the precipitate was taken and placed on a glass plate. When the liquid metal slurry on the glass plate contacts the air-water interface, the liquid metal particles automatically diffuse into the interface. After the film in the interface is saturated, the glass plate is removed to obtain a self-assembled microparticle film. Place the object below the water surface and slowly lift it up vertically. The self-assembled film at the interface will automatically attach to the surface of the object.

Preparation of conformal devices on the human skin

All wearable electronic experiments in this paper are carried out in the hands of the first author with his written consent. Firstly, paste a stickers-based mask on the surface of the finger. Then, insert the finger into the beaker that has been prepared with LMPM. The conformal liquid metal particle film attached to the surface of the finger can be obtained by slowly lifting the finger from water. After activating the film with a brush, the mask is removed, and finally a conformal liquid metal device on the skin surface is obtained. A multimeter is used for subsequent electrical tests.

DATA AVAILABILITY

The data that support the findings of this study are available from the corresponding author upon reasonable request.

REFERENCES

1. Sim, K. et al. Three-dimensional curvy electronics created using conformal additive stamp printing. *Nat. Electron.* **2**, 471–479 (2019).
2. Jung, D. et al. Highly conductive and elastic nanomembrane for skin electronics. *Science* **373**, 1022–1026 (2021).
3. Kim, D. H. et al. Epidermal electronics. *Science* **333**, 838 (2011).
4. Yang, J. C. et al. Electronic skin: Recent progress and future prospects for skin-attachable devices for health monitoring, robotics, and prosthetics. *Adv. Mater.* **31**, e1904765 (2019).
5. Wang, C., Wang, C., Huang, Z. & Xu, S. Materials and structures toward soft electronics. *Adv. Mater.* **30**, e1801368 (2018).
6. Rogers, J. A. Materials and mechanics for stretchable electronics. *Science* **327**, 1603 (2010).
7. Xue, Z., Song, H., Rogers, J. A., Zhang, Y. & Huang, Y. Mechanically-guided structural designs in stretchable inorganic electronics. *Adv. Mater.* **32**, e1902254 (2020).
8. Wu, H. et al. Fabrication techniques for curved electronics on arbitrary surfaces. *Adv. Mater. Tech.* **5**, 2000093 (2020).
9. Dickey, M. D. Stretchable and soft electronics using liquid metals. *Adv. Mater.* **29**, 1606425 (2017).
10. Lee, G. H. et al. A personalized electronic tattoo for healthcare realized by on-the-spot assembly of an intrinsically conductive and durable liquid-metal composite. *Adv. Mater.* **34**, e2204159 (2022).
11. Ding, L. et al. In situ deposition of skin-adhesive liquid metal particles with robust wear resistance for epidermal electronics. *Nano Lett.* **22**, 4482–4490 (2022).
12. Daeneke, T. et al. Liquid metals: fundamentals and applications in chemistry. *Chem. Soc. Rev.* **47**, 4073 (2018).
13. Kazem, N., Hellebrekers, T. & Majidi, C. Soft multifunctional composites and emulsions with liquid metals. *Adv. Mater.* **29**, 1605985 (2017).
14. Chen, S., Wang, H.-Z., Zhao, R.-Q., Rao, W. & Liu, J. Liquid metal. *Compos., Matter* **2**, 1446–1480 (2020).
15. Wang, X. et al. Soft and moldable Mg-doped liquid metal for conformable skin tumor photothermal therapy. *Adv. Healthc. Mater.* **7**, e1800318 (2018).
16. Dong, R. et al. Printed stretchable liquid metal electrode arrays for in vivo neural recording. *Small* **17**, e2006612 (2021).
17. Dong, R. et al. Highly stretchable metal-polymer conductor electrode array for electrophysiology. *Adv. Healthc. Mater.* **10**, e2000641 (2021).
18. Bark, H. & Lee, P. S. Surface modification of liquid metal as an effective approach for deformable electronics and energy devices. *Chem. Sci.* **12**, 2760–2777 (2021).
19. Moon, G. D. et al. Assembled monolayers of hydrophilic particles on water surfaces. *ACS Nano* **5**, 8600–8612 (2011).
20. Lin, Y., Genzer, J. & Dickey, M. D. Attributes, fabrication, and applications of gallium-based liquid metal particles. *Adv. Sci.* **7**, 2000192 (2020).
21. Song, H. et al. Ga-based liquid metal micro/nanoparticles: recent advances and applications. *Small* **16**, e1903391 (2020).
22. Xu, Y., Konrad, M. P., Lee, W. W., Ye, Z. & Bell, S. E. A method for promoting assembly of metallic and nonmetallic nanoparticles into interfacial monolayer films. *Nano Lett.* **16**, 5255–5260 (2016).
23. Pekdemir, S. et al. Chemical funneling of colloidal gold nanoparticles on printed arrays of end-grafted polymers for plasmonic applications. *ACS Nano* **14**, 8276–8286 (2020).
24. Xiao, P. et al. Hydrophilic/hydrophobic interphase-mediated bubble-like stretchable janus ultrathin films toward self-adaptive and pneumatic multifunctional electronics. *ACS Nano* **13**, 4368–4378 (2019).
25. Guan, Y. et al. Air/water interfacial assembled rubbery semiconducting nanofilm for fully rubbery integrated electronics. *Sci. Adv.* **6**, eabb356 (2020).
26. Song, L. et al. Instant interfacial self-assembly for homogeneous nanoparticle monolayer enabled conformal "lift-on" thin film technology. *Sci. Adv.* **7**, eabk2852 (2021).
27. Song, C. et al. Large-area nanosphere self-assembly monolayers for periodic surface nanostructures with ultrasensitive and spatially uniform SERS sensing. *Small* **18**, e2104202 (2022).
28. Chang, J., Lee, J., Georgescu, A., Huh, D. & Kang, T. Generalized on-demand production of nanoparticle monolayers on arbitrary solid surfaces via capillary-mediated inverse transfer. *Nano Lett.* **19**, 2074–2083 (2019).
29. Huang, Y. et al. Assembly and applications of 3D conformal electronics on curvilinear surfaces. *Mater. Horiz.* **6**, 642–683 (2019).
30. Gao, P. et al. Large-area nanosphere self-assembly by a micro-propulsive injection method for high throughput periodic surface nanotexturing. *Nano Lett.* **15**, 4591–4598 (2015).
31. Scanlon, M. D., Smirnov, E., Stockmann, T. J. & Peljo, P. Gold nanofilms at liquid-liquid interfaces: An emerging platform for redox electrocatalysis, nanoplasmonic sensors, and electrovariable optics. *Chem. Rev.* **118**, 3722–3751 (2018).
32. Shin, Y., Song, J., Kim, D. & Kang, T. Facile preparation of ultrasmall void metallic nanogap from self-assembled gold-silica core-shell nanoparticles monolayer via kinetic control. *Adv. Mater.* **27**, 4344–4350 (2015).
33. Das Gupta, T. et al. Self-assembly of nanostructured glass metasurfaces via templated fluid instabilities. *Nat. Nanotechnol.* **14**, 320–327 (2019).
34. Liu, D., Cai, W., Marin, M., Yin, Y. & Li, Y. Air-liquid interfacial self-assembly of two-dimensional periodic nanostructured arrays. *ChemNanoMat* **5**, 1338–1360 (2019).
35. Thrasher, C. J., Farrell, Z. J., Morris, N. J., Willey, C. L. & Tabor, C. E. Mechanoresponsive polymerized liquid metal networks. *Adv. Mater.* **31**, e1903864 (2019).

AUTHOR CONTRIBUTIONS

(1) Substantial contributions to the conception of the work and the acquisition, analysis of the data: F. L., W. L., X. L., F. X., R.-W. L., (2) Drafting the work or revising it critically for important intellectual content: F. L., Z. H., W. L., Y. L., R.-W. L., (3) Final approval of the completed version, Y. W., J. S., Y. L., R.-W. L., (4) Accountability for all aspects of the work in ensuring that questions related to the accuracy or integrity of any part of the work are appropriately investigated and resolved: Z. H., J. L., H. Y., Y. W., S. L., Y. L., R.-W. L.

COMPETING INTERESTS

The authors declare no competing interests.

ADDITIONAL INFORMATION

Supplementary information The online version contains supplementary material available at https://doi.org/10.1038/s41528-023-00263-2.

Correspondence and requests for materials should be addressed to Yiwei Liu or Run-Wei Li.

Reprints and permission information is available at http://www.nature.com/reprints

Publisher's note Springer Nature remains neutral with regard to jurisdictional claims in published maps and institutional affiliations.